

## In vivo detection and imaging of phosphatidylserine expression during programmed cell death

FRANCIS G. BLANKENBERG\*,†, PETER D. KATSIKIS‡, JONATHAN F. TAIT§, R. ERIC DAVIS¶, LOUIS NAUMOVSKI||, KATSUICHI OHTSUKI†, SUSAN KOPIWODA†, MICHAEL J. ABRAMS\*\*, MARILYN DARKES\*\*, ROBERT C. ROBBINS††, HOLDEN T. MAECKER‡‡, AND H.W. STRAUSS†

\*Department of Radiology, †Department of Genetics, §Department of Pathology, ||Department of Pediatrics (Hematology/Oncology), ††Department of Cardiothoracic Surgery, ‡Department of Medicine/Oncology, Stanford University School of Medicine, 300 Pasteur Drive, Stanford, CA 94305-5105; §Department of Laboratory Medicine, University of Washington, Health Sciences, Room NW-120, Box 357110, Seattle, WA 98195-7110; and \*\*Anor MED Incorporated, 20353 64th Avenue, Suite #100, Langley, British Columbia, Canada V3A 7R3

Communicated by Victor A. McKusick, Johns Hopkins University, Baltimore, MD, March 6, 1998 (Received for review January 27, 1998)

**ABSTRACT** One of the earliest events in programmed cell death is the externalization of phosphatidylserine, a membrane phospholipid normally restricted to the inner leaflet of the lipid bilayer. Annexin V, an endogenous human protein with a high affinity for membrane bound phosphatidylserine, can be used *in vitro* to detect apoptosis before other well described morphologic or nuclear changes associated with programmed cell death. We tested the ability of exogenously administered radiolabeled annexin V to concentrate at sites of apoptotic cell death *in vivo*. After derivatization with hydrazinonicotinamide, annexin V was radiolabeled with technetium 99m. *In vivo* localization of technetium 99m hydrazinonicotinamide-annexin V was tested in three models: fumant hepatic apoptosis induced by anti-Fas antibody injection in BALB/c mice; acute rejection in ACI rats with transplanted heterotopic PVG cardiac allografts; and cyclophosphamide treatment of transplanted 38C13 murine B cell lymphomas. External radionuclide imaging showed a two- to sixfold increase in the uptake of radiolabeled annexin V at sites of apoptosis in all three models. Immunohistochemical staining of cardiac allografts for exogenously administered annexin V revealed intense staining of numerous myocytes at the periphery of mononuclear infiltrates of which only a few demonstrated positive apoptotic nuclei by the terminal deoxynucleotidyltransferase-mediated UTP end labeling method. These results suggest that radiolabeled annexin V can be used *in vivo* as a noninvasive means to detect and serially image tissues and organs undergoing programmed cell death.

Programmed cell death (apoptosis) plays a crucial role in the pathogenesis of a number of disorders including AIDS and other viral illnesses, cerebral and myocardial ischemia, autoimmune and neurodegenerative diseases, organ and bone marrow transplant rejection, and tumor response to chemotherapy and radiation (1–3). Since the original description of apoptosis by Wyllie in 1972, its assessment *in vivo* has required direct examination of biopsied or aspirated material (4). An imaging technique capable of localizing and quantifying apoptosis *in vivo* would permit assessment of disease progression or regression and similarly define the efficacy of therapy designed to inhibit or induce cell death (5–6).

Cells undergoing apoptosis redistribute phosphatidylserine (PS) from the inner leaflet of the plasma membrane lipid bilayer to the outer leaflet (7, 8). The externalization of PS is a general feature of apoptosis occurring before membrane bleb formation and DNA degradation (7, 8). Annexin V, a human

protein with a molecular weight of 36,000 has a high affinity for cell or platelet membranes with exposed PS *in vitro* and *in vivo* (9–13). This observation has led to testing radiolabeled annexin V in animal models of acute thrombosis and imaging of atrial thrombi in patients with atrial fibrillation (14, 15). In the current study, annexin V was derivatized with hydrazinonicotinamide (HYNIC) and coupled to technetium 99m (<sup>99m</sup>Tc) (16) before i.v. administration in animal models of apoptosis. HYNIC, an nicotinic acid analog, is a bifunctional molecule capable of bonding to lysine residues of proteins on one moiety and conjugates of <sup>99m</sup>Tc on the other. The agent forms stable complexes with proteins (16) without affecting bioactivity. We performed scintigraphic imaging studies with derivatized annexin V to determine its ability *in vivo* to detect sites of apoptotic cell death occurring in Fas-mediated hepatocyte apoptosis, acute cardiac allograft rejection, and cyclophosphamide treatment of B cell lymphoma. Such *in vivo* imaging may prove useful in the clinical setting for noninvasive diagnosis, monitoring of disease progression or regression, and determining efficacy of treatment.

### MATERIALS AND METHODS

**Preparation of <sup>99m</sup>Tc HYNIC-Annexin V.** Human annexin V was produced by expression in *Escherichia coli* as described (13, 17, 18); this material retains PS-binding activity equivalent to that of native annexin V (18). Concentrations were determined using  $E_{280} = 0.6 \text{ ml/mg}^{-1} \text{ cm}^{-1}$  and molecular weight was taken as 35,806. HYNIC-derivatized annexin V was produced by the gentle mixing of 5.6 mg/ml of annexin V in 20 mM Hepes, pH 7.4, and 100 mM NaCl for 3 hr shielded from light with succinimidyl 6-HYNIC (Anor Med, Langley, British Columbia) [222 µg in 18.5 µl (42 mM solution) of *N,N*-dimethyl formamide] at room temperature. The reaction was quenched with 500 µl of 500 mM glycine in PBS, pH 7.4, and then dialyzed at 4°C against 20 mM sodium citrate, pH 5.2, and 100 mM NaCl overnight. Precipitate was then removed by centrifugation at 15,000 × g for 10 min. Then, 100 µl (100 µg) aliquots of HYNIC-annexin V were stored at –70°C. Incorporation of HYNIC into annexin V was found to be 0.9 mol/mol of annexin V by using the methods of King *et al.* (19). Membrane-binding activity of HYNIC-annexin V and decayed <sup>99m</sup>Tc HYNIC-annexin V was determined by a modified competition assay in which 5 nmol/liter fluorescein isothiocyanate (FITC)-annexin V was substituted for <sup>125</sup>I-annexin V (12, 17). After incubation for 15 min at room temperature, cells

The publication costs of this article were defrayed in part by page charge payment. This article must therefore be hereby marked "advertisement" in accordance with 18 U.S.C. §1734 solely to indicate this fact.

© 1998 by The National Academy of Sciences 0027-8424/98/956349-6\$2.00/0  
PNAS is available online at <http://www.pnas.org>.

Abbreviations: TUNEL, terminal deoxynucleotidyltransferase-mediated UTP end labeling; PS, phosphatidylserine; HYNIC, hydrazinonicotinamide; <sup>99m</sup>Tc, technetium 99m; FITC, fluorescein isothiocyanate; HSA, human serum albumin; ROI, region of interest.

\*To whom reprint requests should be addressed. e-mail: MA.FRB@Forsythe.Stanford.Edu.

were centrifuged, the FITC-annexin V bound to the pelleted cells was released with EDTA, and the released FITC-annexin V was measured by fluorometry. In this assay system, unmodified annexin V, HYNIC-annexin V, and decayed  $^{99m}$ Tc HYNIC-annexin V inhibited 50% of the binding of FITC-annexin V at concentrations of 8 nmol/liter, 10.5 nmol/liter, and 12.3 nmol/liter, respectively.

To bind  $^{99m}$ Tc to the HYNIC-annexin conjugate 80  $\mu$ l of stannous chloride (50 mg/ml in 0.1 M HCl purged for 2 hr with N<sub>2</sub> gas) was first added to 50 ml of a 20 mM tricine solution (pH 7.1, purged for 1 hr with N<sub>2</sub> gas; tricine = N-[tris(hydroxymethyl)methyl]glycine). Two hundred microliters of the Sn-tricine solution was then added to 100  $\mu$ l of  $^{99m}$ Tc O<sub>4</sub> (4–20 mCi (1 Ci = 37 GBq) activity in 0.9% NaCl) previously mixed with a 100  $\mu$ l (100  $\mu$ g) aliquot of HYNIC-annexin V according to the methods described by Abrams *et al.* (20). Specific activity was 10–200  $\mu$ Ci/ $\mu$ g protein (depending on desired activity) with a radiopurity of 92–97% determined with instant thin layer chromatography using 0.9% saline solution as a solvent.

**Scintillation Well Counting.** Samples were counted in a Packard Cobra II gamma counter (Packard). The energy window was set at a lower level of 120 keV and an upper level of 170 keV for  $^{99m}$ Tc. When  $^{125}$ I was counted, samples were allowed to decay for at least 24 hr. The samples were then recounted using both the technetium window and an  $^{125}$ I setting with a lower level of 20 keV and an upper level of 50 keV. Samples were corrected for any residual cross talk.

**Radionuclide Imaging.** A Technicare 420 mobile camera (Technicare, Solon, OH) equipped with a low energy high resolution parallel hole collimator was used to record the radionuclide distribution in mice and rats sedated with a mixture of 80 mg/kg ketamine and 4 mg/kg acepromazine injected i.m. Data were recorded by using a 20% window centered on the 140 keV photopeak of technetium into a 128  $\times$  128 matrix of a dedicated computer system for digital display and analysis (ICON, Siemens, Hoffman Estates, IL). All images were recorded for a preset time of 10–15 min.

**Murine Model of Fas-Mediated Apoptosis.** Massive hepatic apoptosis can be induced within 1–2 hr in mice following i.v. injection of anti-Fas antibody (21). We used this well described model of *in vivo* programmed cell death to test the specific localization of  $^{99m}$ Tc HYNIC-annexin to an organ undergoing apoptosis *in vivo*. Four- to five-wk-old BALB/c mice were injected i.v. with purified hamster anti-Fas mAb (Jo2, 10  $\mu$ g/animal, PharMingen, San Diego, CA) using the model proposed by Ogasawara *et al.* (21). Mice were then injected i.v. with 25–50  $\mu$ g/kg of  $^{99m}$ Tc HYNIC-annexin V (10–25  $\mu$ Ci/animal for biodistribution study and 100–150  $\mu$ Ci/animal for imaging studies) 1 or 2 hr after antibody treatment. Animals were killed 1 hr after administration of radiopharmaceutical followed by organ removal for scintillation counting of radioactivity and for histologic and immunohistochemical analyses.

Control studies with  $^{99m}$ Tc labeled human serum albumin (HSA) also were performed in untreated and anti-Fas treated mice. Although other proteins were considered as controls, albumin was selected because distinguishing the potential vascular disruption and protein leakage associated with acute apoptosis was a major goal of this control experiment. The animals were injected with 100–150  $\mu$ Ci of  $^{99m}$ Tc labeled HSA (25 mg/animal) and imaged at 1 and 2 hr, in similar fashion to the mice receiving  $^{99m}$ Tc HYNIC-annexin.

**Rodent Model of Cardiac Transplantation.** Adult male ACI rats (250–350 g) received heterotopic cardiac allografts from PVG donors (obtained from Harlan-Sprague-Dawley) anastomosed to the hosts' abdominal aorta and inferior vena cava according to a modification of the technique of Ono and Lindsey (22). Syngeneic cardiac isografts from ACI donors also were transplanted to the abdomens of host ACI rats. PVG cardiac allografts in ACI recipients using the model above begin to undergo rejection between 4 and 5 days post-

transplantation as assessed by decreased pulsation to palpation. Five days after transplantation all of the animals received 700–900  $\mu$ Ci of  $^{99m}$ Tc HYNIC-annexin V (10–20  $\mu$ g protein/kg) via tail vein and were imaged 1 hr later. Animals were then killed, and native and transplanted hearts underwent scintillation counting and histopathologic studies.

**Murine Model of Lymphoma.** 38C13 murine B cell lymphomas (23) were grown in C3H/HeN mice (Harlan Breeders, Indianapolis) following s.c. injection of 400 tumor cells suspended in 200  $\mu$ l of RPMI medium 1640 (without serum) into the left flank. Fourteen days after implantation mice underwent treatment with 100 mg/kg of cyclophosphamide injected i.p. Mice were injected i.v. with 25–50  $\mu$ g/kg of  $^{99m}$ Tc HYNIC-annexin V (100–150  $\mu$ Ci/animal) 20 hr after cyclophosphamide administration. Animals were then imaged and killed 1 hr after injection of radiopharmaceutical after tumor removal for scintillation counting and histopathologic studies.

**Immunostaining for Bound Human Annexin V and Apoptotic Nuclei.** Formalin-fixed paraffin-embedded tissues were sectioned at 5  $\mu$ m for staining with hematoxylin/eosin or other techniques. Immunostaining for bound human annexin V was performed with a rabbit anti-serum raised against human placental annexin V and affinity purified with recombinant annexin V coupled to Affi-Gel (Bio-Rad). Immunohistochemical detection then was completed by sequential incubations with biotin-labeled goat anti-rabbit antibody and avidin-horseradish peroxidase complex (Jackson Immuno Research), followed by reaction with 3,3'-diaminobenzidine as described by Bindl and Warnke (24).

For the detection of apoptotic nuclei, sections were stained using a modification of the terminal deoxynucleotidyltransferase-mediated UTP end labeling (TUNEL) method described by Gavrieli *et al.* (25). After inhibition of endogenous peroxidase, deparaffinized sections were digested with proteinase K (20  $\mu$ g/ml) for 15 min at room temperature. Sections were then incubated with  $\lambda$  exonuclease (Life Technologies, Gaithersburg, MD) at 5 unit/ml for 30 min at 37°C followed by equilibration with terminal deoxynucleotidyltransferase reaction buffer (0.2 M potassium cacodylate, 25 mM Tris-HCl, 0.25 mg/ml BSA, 1.5 mM CaCl<sub>2</sub>, 20 mg/ml polyvinylpyrrolidone, and 20 mg/ml Ficoll) and 5  $\mu$ M dATP. The end-labeling reaction then was performed in terminal deoxynucleotidyltransferase reaction buffer also containing a final concentration of 75 unit/ml of terminal deoxynucleotidyltransferase and 100  $\mu$ M of 1,N-6-ethenol-dATP (Sigma). After a 60-min incubation at 37°C, the reaction was quenched via rinsing with 1  $\times$  SSC (standard saline citrate). Sections were then incubated with murine 1G4 mAb (gift from Regina Santella, Columbia University), which recognizes the ethenoadenine moiety (26). Subsequent immuno-histochemical detection was as described above, using a biotin-labeled goat anti-mouse antibody.

## RESULTS

**Biodistribution of Radiolabeled Annexin V in Fulminant Hepatic Apoptosis.** There was a 134% and 304% increase in the hepatic uptake of  $^{99m}$ Tc HYNIC-annexin V above controls at 1 and 2 hr after anti-Fas antibody injection, respectively, as determined by biodistribution studies (Table 1). Hepatic uptake was inversely proportional to renal uptake in treated mice with a 75% decrease in renal activity 2 hr after treatment. Of note, there was <5% excretion of administered radiopharmaceutical into the urine in control or treated animals. Splenic uptake was 108% and 54% above control values in the 1- and 2-hr treatment groups, respectively.

Subgroups of mice were co-injected with  $^{125}$ I-HSA to control for nonspecific uptake of inert protein from the circulation caused by hepatic endothelial cell breakdown (27). Hepatic uptake was 120% above control values at 1 hr after anti-Fas antibody injection and remained unchanged in contrast to the

Table 1. Biodistribution study of radiolabeled annexin V after anti-Fas antibody treatment

	<sup>99m</sup> Tc	Controls (n = 9)	1-hr anti-Fas (n = 15)	2-hr anti-Fas (n = 12)
A)	% ID			
	Liver	12.2 ± 1.4	28.6 ± 9.4**	49.3 ± 12.7***
	Kidneys	55.9 ± 8.9	35.2 ± 14.4**	14.0 ± 10.0***
B)	<sup>125</sup> I	Controls	1-hr anti-Fas (n = 6)	2-hr anti-Fas (n = 5)
	% ID	(n = 4)		
	Liver	3.98 ± 1.09	8.77 ± 3.53*	8.4 ± 1.92*
C)	Kidneys	1.37 ± 0.35	1.88 ± 0.37(ns)	1.82 ± 0.38(ns)
	Spleen	0.39 ± 0.09	0.47 ± 0.15(ns)	0.37 ± 0.041(ns)
	Weight (grams)	Controls (n = 9)	1-hr anti-Fas (n = 15)	2-hr anti-Fas (n = 12)
	Liver	1.06 ± 0.097	1.29 ± 0.32(ns)	1.37 ± 0.22*
	Kidneys	0.31 ± 0.061	0.32 ± 0.079(ns)	0.37 ± 0.072(ns)
	Spleen	0.12 ± 0.022	0.12 ± 0.02(ns)	0.11 ± 0.014(ns)

% injected dose (ID) per organ corrected for background, decay, and tail infiltration are listed for mice injected with 100–150  $\mu$ Ci (radiopurity >95%, specific activity 150–200  $\mu$ Ci/ $\mu$ g protein) of <sup>99m</sup>Tc HYNIC-annexin co-injected with 0.6  $\mu$ Ci (25 mg) of <sup>125</sup>I radiolabeled HSA. A) Biodistribution of <sup>99m</sup>Tc HYNIC-annexin V, B) <sup>125</sup>I-HSA, and C) Organ weight. Data are expressed as mean ± standard error of the mean. P-values are shown in parenthesis () for Dunnett's test for multiple comparison of means of the 1- or 2-hr post-treatment groups compared with control. ns, not significant (i.e., P-value > 0.05); \*, P < 0.05; \*\*, P < 0.001; \*\*\*, P < 0.0001.

progressive rise in annexin V uptake. There was a 29% increase in liver weight at 2 hr. Renal and splenic weight and uptake of <sup>125</sup>I-HSA did not change significantly after treatment.

Sections of livers from mice treated with anti-Fas antibody showed a spectrum of nuclear changes characteristic of apoptosis (margination of chromatin, pyknosis, and karyorrhexis) as early as 1 hr after injection; changes were more pronounced and focally associated with hemorrhage (peliosis) 2 hr after treatment (Fig. 1A). Immunostaining for <sup>99m</sup>Tc HYNIC-annexin V was observed at the cytoplasmic border of apoptotic hepatocytes; although this result was focal, the localization pattern is consistent with PS externalization, and staining never was observed in normal hepatocytes (Fig. 1B) or in anti-Fas antibody-treated mice not injected with <sup>99m</sup>Tc HYNIC-annexin V (data not shown).

**In Vivo Imaging of Fas-Mediated Fulminant Hepatic Apoptosis.** A high concentration of radiolabeled annexin V activity was observed by scintillation camera imaging in the kidneys of control animals with minimal concentration in other organs (Fig. 2). Hepatic uptake in control mice [12% of injected dose (% ID)] did not permit clear delineation of the liver. In mice treated with anti-Fas antibody, there was a diffuse increase in the intensity of hepatic uptake of <sup>99m</sup>Tc HYNIC-annexin V observed at 1 hr, which continued to rise at 2 hr after treatment. The transient increase in splenic uptake and the fall in renal activity found in the biodistribution studies both were visualized readily with external imaging following anti-Fas treatment. A total of 19 mice (six control, seven 1-hr, and six 2-hr anti-Fas-treated animals) underwent biodistribution study after imaging with <sup>99m</sup>Tc HYNIC-annexin V. The percentage of whole body activity per organ determined by region of interest (ROI) image analysis correlated well with the percentage of injected dose per organ determined by biodistribution (linear correlation coefficients for the liver, kidney, and spleen of  $r^2 = 0.853, 0.860$ , and  $0.979$ , respectively.)

There was no perceptible difference in liver, renal, or splenic uptake on the <sup>99m</sup>Tc-HSA images between the treated mice and controls (images not shown). There also was a direct correlation of observed uptake of <sup>99m</sup>Tc-HSA as seen by ROI image analysis and the biodistribution of <sup>99m</sup>Tc-HSA (data not shown), which mirrored the biodistribution of <sup>125</sup>I-HSA.

**In Vivo Imaging of Cardiac Allograft Rejection.** All of the PVG cardiac allografts ( $n = 4$ ) were visualized easily with <sup>99m</sup>Tc HYNIC-annexin V 5 days after transplantation (Fig. 3).

ACI syngeneic cardiac isografts ( $n = 3$ ) had no visible activity after injection of <sup>99m</sup>Tc HYNIC-annexin with uptakes of

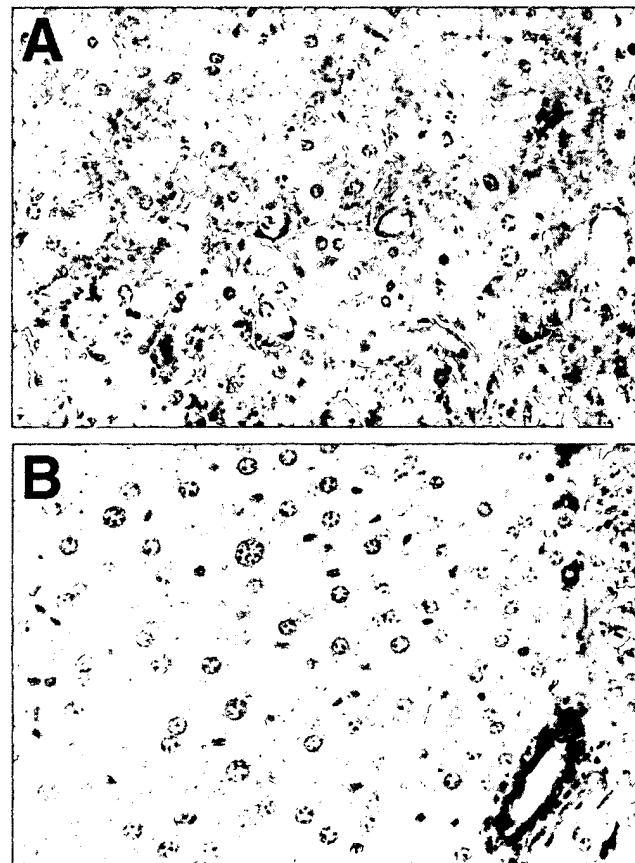


FIG. 1. Histologic sections of murine liver immunostained for exogenously administered human annexin V. (A) Two hours after anti-Fas antibody treatment there is extensive apoptotic nuclear change, slight cytoplasmic retraction, and interstitial hemorrhage. Annexin V staining (brown immunostaining product) is focally present at the cytoplasmic border of apoptotic hepatocytes. (B) No hepatocyte staining was observed in untreated mice. Staining of bile duct epithelium was caused by antibody cross-reactivity because it also was seen in the absence of exogenously administered human annexin V (data not shown). (Diaminobenzidine immunostain with hematoxylin counterstain,  $\times 40$  objective magnification.)

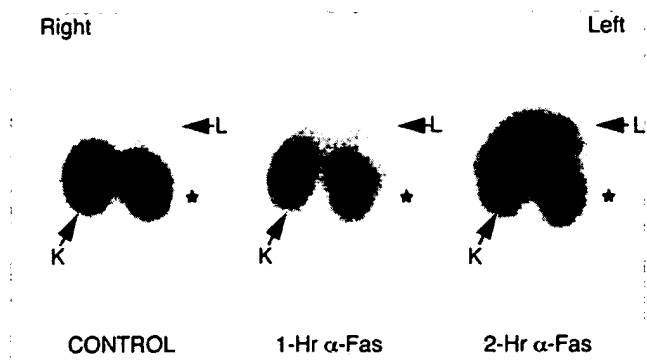


FIG. 2. Imaging Fas-mediated fulminant hepatic apoptosis with radiolabeled annexin V. One hour after injection of  $150 \mu\text{Ci}$  of radiopharmaceutical ( $50 \mu\text{g}/\text{kg}$  of protein) mice were imaged in the prone anterior projection. There was a progressive increase in  $^{99m}\text{Tc}$  annexin V uptake of the liver of mice at 1 and 2 hr after anti-Fas antibody injection. Liver activity (L) was 111% and 239% above control values in the 1- and 2-hr mice, respectively, as shown by region of interest image analysis. Kidney activity (K) was 70% and 64% below control values in the 1- and 2-hr mice, respectively. Splenic activity (\*) was 168% and 45% above control values in the 1- and 2-hr mice, respectively.

radiopharmaceutical identical to native cardiac activity as confirmed by scintillation well counting (data not shown). The percentage of whole body activity of PVG allografts was 213% above ACI isograft activity ( $P < 0.005$ ; using a two-tailed student's *t* test) determined by ROI image analysis. Scintillation well-counting assay revealed a  $>11$ -fold increase in  $^{99m}\text{Tc}$  HYNIC-annexin V uptake in PVG allografts as compared with native heart activity.

Sections of PVG cardiac allografts 5 days after transplantation showed a marked mononuclear inflammatory cell infiltrate in all animals; no infiltrate was observed in syngeneic or native hearts. The infiltrate surrounded areas of myocardial injury and was associated with thrombosis of myocardial vessels. In the center of these areas, there was frank necrosis, with no staining by hematoxylin, but at the periphery, there were nuclei with changes of apoptosis as confirmed by TUNEL

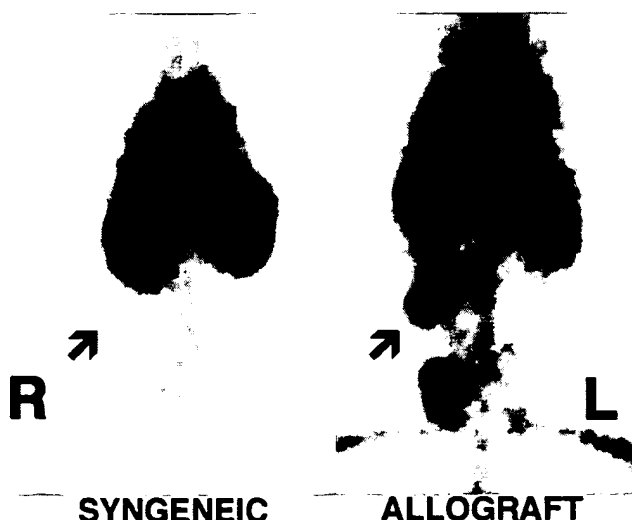


FIG. 3. Imaging cardiac allograft rejection with radiolabeled annexin V. Representative images of abdominal cardiac syngeneic ACI isograft and PVG allograft in ACI host rats 5 days after transplantation. Rats were imaged in the prone anterior projection 1 hr after injection with  $900 \mu\text{Ci}$  of  $^{99m}\text{Tc}$ -annexin V. Location of transplanted hearts are marked by arrows. Intense uptake of  $^{99m}\text{Tc}$  HYNIC-annexin V was observed in the cardiac allograft animal (Right) as compared with the lack of visualization of the syngeneic cardiac isograft (Left).

staining (Figs. 4A and B). Immunostaining for  $^{99m}\text{Tc}$  HYNIC-annexin V was observed in a granular pattern in cardiac myocytes at the junction of inflamed and necrotic areas; the nuclei of these cells were stained still by hematoxylin, further suggesting that they were apoptotic rather than necrotic (Fig. 5A). Anti-annexin V staining was far more extensive in terms of the number of positive myocytes and intensity compared with TUNEL. Anti-annexin staining was heavy and clumped in frankly necrotic areas as expected (Fig. 5A) but was specific; no staining was observed in syngeneic or native hearts or in staining of allografted hearts in which the primary antibody was omitted (Fig. 5B).

**In Vivo Imaging of Treated Murine Lymphoma.** Untreated flank tumor implants ( $n = 8$ ) were seen easily by scintillation camera imaging (Fig. 6) and had an annexin V uptake 365% above normal soft tissue activity as shown by ROI image analysis. Treated flank tumors ( $n = 6$ ) showed readily visualizable increases in  $^{99m}\text{Tc}$  HYNIC annexin V activity of 78% above control values expressed as whole body activity per gram of tumor ( $P < 0.05$  using a two-tailed student's *t* test for significance). This result was confirmed by scintillation well counting in which treated tumors demonstrated a 132% increase in annexin V uptake expressed as percentage of injected dose per gram of tumor ( $P < 0.05$ ) with a 58% fall in weight ( $P < 0.05$ ) compared with the control. The whole body activity per gram of tumor as seen by ROI image analysis linearly correlated to percentage of injected dose per gram of tumor determined on biodistribution study ( $r^2 = 0.831$ ). Histologic

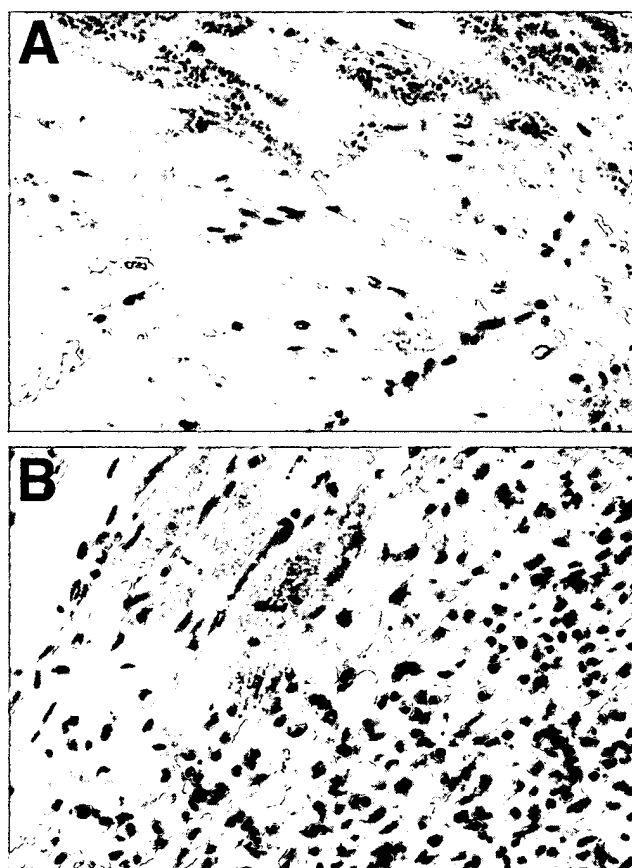


FIG. 4. Staining for apoptotic nuclei in allografted rodent heart 5 days after transplantation. (A) TUNEL staining showing apoptotic nuclei and fragments in some myocytes bordering areas of necrosis (myocytes without visible nuclei in upper half of field). (B) TUNEL positive nuclei and fragments within inflammatory infiltrate (right half of field) and in some myocytes bordering regions of inflammation. (Diaminobenzidine immunostain with hematoxylin counterstain,  $\times 40$  objective magnification.)

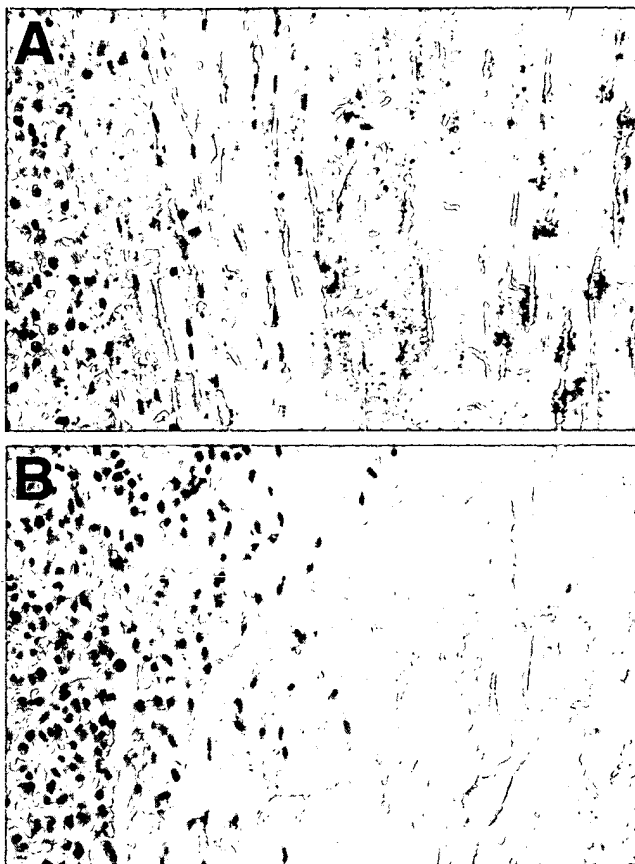


FIG. 5. Immunostaining for exogenously administered human annexin V in allografted rodent heart 5 days after transplantation. (A) Immunostaining with an antibody to human annexin V shows dense, granular staining of apoptotic myocytes at the periphery of the inflammatory infiltrate. Staining of necrotic myocytes (myocytes without visible nuclei) was clumped heavily and central. (B) Immunostaining of area similar to that shown in A omitting the primary antibody, shows no reaction product. (Diaminobenzidine immunostain with hematoxylin counterstain,  $\times 40$  objective magnification.)

analysis demonstrated virtually complete ( $>95\%$ ) apoptosis of all lymphoblasts in treated tumors with  $<5\%$  apoptotic cells in controls (data not shown).

## DISCUSSION

These experiments indicate that exposure of PS on the surface of cells undergoing apoptosis can be detected *in vivo* with radiolabeled annexin V in animal models including Fas-mediated fulminant hepatitis, cardiac allograft rejection, and tumor response to treatment.  $^{99m}\text{Tc}$  HYNIC-labeled annexin V radionuclide imaging demonstrated clear and specific localization to regions of apoptotic cell death. As has been shown for annexin V reagents *in vitro*, annexin V radionuclide imaging can provide a tool which can directly assess for early stages of programmed cell death, before membrane vesicle formation and DNA degradation particularly as measured by the TUNEL method (7, 8). Imaging of tissues undergoing apoptosis could be helpful in monitoring the efficacy of therapy of diseases associated with abnormal induction or inhibition of programmed cell death. Apoptosis appears to play an important role in autoimmune and neurodegenerative diseases, cardiomyopathy, myocarditis, cerebral and myocardial ischemia, infectious diseases, cancer, viral induced hepatitis, and organ and bone marrow transplant rejection (1).

The numerous anti-annexin V positive-staining myocytes found in rejecting rodent heart transplants with nuclei which

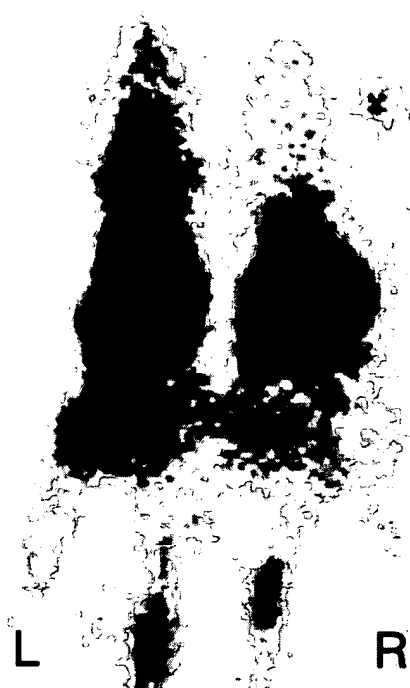


FIG. 6. Imaging treated murine lymphoma with radiolabeled annexin V. CH3. HeN mice 14 days after implantation of 38C13 murine B cell lymphoma s.c. into the left flank were treated with 100 mg/kg of cyclophosphamide injected i.p. Twenty hours after treatment mice were injected with 150  $\mu\text{Ci}$  of  $^{99m}\text{Tc}$  HYNIC annexin V (50  $\mu\text{g}/\text{kg}$  of protein). One hour after administration of  $^{99m}\text{Tc}$  HYNIC annexin V mice were imaged in the prone anterior projection. Treated tumor demonstrated uptakes of 363% and 454% above control seen by region of interest analysis and biodistribution assay, respectively. Control tumor weight = 1.29 grams, treated tumor weight = 0.82 grams. L, left; R, right.

were only occasionally TUNEL positive implies that radiolabeled annexin V imaging may be superior to standard histopathologic assessments of apoptosis. These data suggests a far greater role for programmed cell death in cardiac allograft rejection than previously reported (28–32). Anti-annexin V staining of apoptotic myocytes (with or without TUNEL stained nuclei) was diffusely granular in appearance in contrast to the peripheral pattern of apoptotic hepatocytes. This pattern of exogenous annexin V localization may relate to the unique cellular morphology of myocardial tissue; the extensive sarcoplasmic reticulum, which communicates with the extracellular space, also may be capable of externalizing PS during apoptosis.

The ability of annexin V to bind to necrotic cells *in vivo* and bind to PS located in the inner leaflet of the plasma membrane is confirmed by finding heavy and clumped anti-annexin V staining in frankly necrotic areas in cardiac allografts. As a result, annexin V localization *in vivo* does not appear to be entirely specific for apoptosis. In the clinical setting, however, the ability of radiolabeled annexin V to noninvasively image both apoptosis and necrosis may prove useful in reducing the need for routine surveillance through endomyocardial biopsy after cardiac transplantation, which currently is the only reliable clinical means to diagnose acute transplant rejection (33, 34). Furthermore, radiolabeled annexin V imaging of the entire myocardium may provide diagnostic information superior to endomyocardial biopsy, which necessarily can only sample a limited region within the right ventricle.

These studies also demonstrate that radiolabeled annexin V imaging can detect an increase in PS exposure associated with apoptosis of implanted murine flank lymphomas after cyclophosphamide treatment. Estimates of the degree of cell death

during the first week of induction therapy using bone marrow aspirates has been shown to provide prognostic information in childhood leukemia (35, 36). Other investigators have shown a direct relationship between the degree of apoptotic cell death and subsequent tumor growth delay in murine models of lymphoma (37, 38). To date, the only noninvasive imaging method shown to detect apoptosis *in vivo* has been lipid proton NMR spectroscopy (5, 6). Lipid proton NMR spectroscopy, however, has inherent problems with magnetic susceptibility outside the central nervous system and has relatively low sensitivity.

Kidneys in control animals have marked uptake of  $^{99m}\text{Tc}$ -HYNIC annexin V. The high renal concentration did not preclude the imaging of other major organs undergoing apoptosis. The cellular site of binding is uncertain, but preliminary autoradiographs suggest the renal distribution of annexin V is cortical. The specific mechanism of renal cortical binding is uncertain but may relate to the intrinsic lipid profile of the kidney, in which there is a significantly higher concentration of PS in the cortex as compared with the papillary regions (39).

The initial increase of  $^{125}\text{I}$ -HSA hepatic uptake after anti-Fas treatment is most likely caused by an expanded extracellular fluid volume from the early breakdown of hepatic endothelial cells as described by Lacronique *et al.* (27) and is confirmed by an increased hepatic weight of these treated animals. The initial increase of  $^{125}\text{I}$ -HSA hepatic uptake, which subsequently remained unchanged, is in marked contrast to the progressive rise of radiolabeled annexin V hepatic uptake, which was specific for increasing numbers of apoptotic hepatocytes.

In summary, this study demonstrates the utility of  $^{99m}\text{Tc}$ -radiolabeled annexin V for *in vivo* imaging of PS expression associated with apoptosis. Serial noninvasive assessments of PS externalization with radiolabeled annexin V may provide a more sensitive and rapid means of monitoring disease progression, determining treatment efficacy, and diagnosing a number of human disorders than is currently possible in the clinical setting.

This work was supported in part by the Child Health Research Fund, Lucile Salter Packard Children's Hospital at Stanford, and by the National Institutes of Health Grant HL-47151. The authors also gratefully acknowledge Dr. Regina Santella for the gift of 1G4 antibody.

- Thompson, B. C. (1995) *Science* **267**, 1456–1462.
- Steller, H. (1995) *Science* **267**, 1445–1449.
- Darzynkiewicz, Z. (1995) *J. Cell. Biochem.* **58**, 151–159.
- Kerr, J. F., Wyllie, A. H. & Currie, A. R. (1972) *Brit. J. Cancer* **26**, 239–257.
- Blankenberg, F. G., Storrs, R. W., Naumovski, L., Goralski, T. & Spielman, D. (1996) *Blood* **87**, 1951–1956.
- Blankenberg, F. G., Katsikis, P. D., Storrs, R. W., Bealieu, C., Spielman, D., Chen, J. Y., Naumovski, L. & Tait, J. F. (1997) *Blood* **89**, 3778–3786.
- Martin, S. J., Reutelingsperger, C. P. M., McGahon, A. J., Rader, J. A., van Schie, R. C. A. A., La Face, D. M. & Green, D. R. (1995) *J. Exp. Med.* **182**, 1545–1556.
- Zwaal, R. F. A. & Schroit, A. (1997) *Blood* **89**, 1121–1132.
- Koopman, G., Reutelingsperger, C. P. M., Kuijten, G. A. M., Keehnen, R. M. J., Pals, S. T. & van Oers, M. H. J. (1994) *Blood* **84**, 1415–1420.

- Verhoven, B., Schlegel, R. A. & Williamson, P. (1995) *J. Exp. Med.* **182**, 1597–1601.
- van Heerde, W. L., de Groot, P. G. & Reutelingsperger, C. P. M. (1995) *Thromb. Haemostasis* **73**, 172–179.
- Tait, J. F. & Gibson, D. (1994) *J. Lab. Clin. Med.* **123**, 741–748.
- Wood, B. L., Gibson, D. F. & Tait, J. F. (1996) *Blood* **88**, 1873–1880.
- Tait, J. F., Cerqueira, M. D., Dewhurst, T. A., Fujikawa, K., Ritchie, J. L. & Stratton, J. R. (1994) *Thromb. Res.* **75**, 491–501.
- Stratton, J. R., Dewhurst, T. A., Kasina, S., Reno, J. M., Cerqueira, M. D., Baskin, D. G. & Tait, J. F. (1995) *Circulation* **92**, 3113–3121.
- Abrams, M. J., Juweid, M., tenKate, C. I., Schwartz, D. A., Hauser, M. M., Gaul, F. E., Fuccello, A. J., Rubin, R. H., Strauss, H. W. & Fischman, A. J. (1990) *J. Nucl. Med.* **31**, 2022–2028.
- Tait, J. F., Engelhardt, S., Smith, C. & Fujikawa, K. (1995) *J. Biol. Chem.* **270**, 21594–21599.
- Tait, J. F. & Smith, C. (1991) *Arch. Biochem. Biophys.* **288**, 141–144.
- King, T. P., Zhao, S. W. & Lam, T. (1986) *Biochemistry* **25**, 5774–5779.
- Larsen, S. K., Solomon, H. F., Caldwell, G. & Abrams, M. J. (1995) *Bioconjugate Chem.* **6**, 635–638.
- Ogasawara, J., Watanabe-Fukunaga, R., Adachi, M., Matsuzawa, A., Kasugai, T., Kitamura, Y., Itoh, N., Suda, T. & Nagata, S. (1993) *Nature (London)* **364**, 806–809.
- Woodley, S. L., Gurley, K. E., Hoffman, S. L., Nicolls, M. R., Hagberg, R., Clayberger, C., Holm, B., Wang, X., Hall, B. M. & Strober, S. (1993) *Transplantation* **56**, 1443–1447.
- Maloney, D. G., Kaminski, M. S., Burowski, D., Haimovich, J. & Levy, R. (1985) *Hybridoma* **4**, 191–209.
- Bindl, J. M. & Warnke, R. A. (1986) *Am. J. Clin. Pathol.* **85**, 490–493.
- Gavrieli, Y., Sherman, Y. & Ben-Sasson, S. (1992) *J. Cell Biol.* **119**, 493–501.
- Young, T. L. & Santella, R. M. (1988) *Carcinogenesis* **9**, 589–592.
- Lacronique, V., Mignon, A., Fabre, M., Viollet, B., Rouquet, N., Molina, T., Porteu, A., Henrion, A., Bouscary, D., Varlet, P., *et al.* (1996) *Nat. Med.* **2**, 80–86.
- Seino, K., Nobuhiko, K., Bashuda, H., Okumura, K. & Yagita, H. (1996) *Int. Immunol.* **8**, 1347–1354.
- Laguens, R. P., Cabeza Meckert, P. M., San Martino, J., Perrone, S. & Favaloro, R. (1996) *J. Heart Lung Transplant.* **15**, 911–918.
- Bergese, S. D., Klenotic, S. M., Wakely, M. E., Sedmak, D. D. & Orosz, C. G. (1997) *Transplantation* **63**, 320–325.
- Jollow, K. C., Sundstrom, J. B., Gravanis, M. B., Kanter, K., Herskowitz, A. & Ansari, A. A. (1997) *Transplantation* **63**, 1482–1489.
- Matiba, B., Mariana, S. M. & Krammer, P. H. (1997) *Immunology* **9**, 59–68.
- Mannaerts, H. F., Simoons, M. L., Balk, A. H., Tijssen, J., van der Borden, S. G., Zondervan, P. E., Mochtar, B., Weimer, W. & Roelandt, J. R. (1993) *J. Heart Lung Transplant.* **12**, 411–421.
- Angermann, C. E., Nassau, K., Stempfle, H-U., Krüger, T. M., Drewello, R., Phys, D., Junge, R., Ing, D., Überfuhr, P., Weib, M., *et al.* (1997) *Circulation* **95**, 140–150.
- Asselin, B. L., Ryan, D., Frantz, C. N., Bernal, S. D., Leavitt, P., Sallan, S. E. & Cohen, H. J. (1989) *Cancer Res.* **49**, 4363–4368.
- Niemeyer, C. M., Gelber, R. D., Tarbell, N. J., Donnelly, M., Clavell, L. A., Blattner, S. R., Donahue, K., Cohen, H. J. & Sallan, S. E. (1991) *Blood* **78**, 2514–2519.
- Stephens, L. C., Hunter, N. R., Ang, K. K., Milas, L. & Meyn, R. E. (1993) *Radiat. Res.* **135**, 75–80.
- Mirkovic, N., Meyn, R. E., Hunter, N. R. & Milas, L. (1994) *Radiother. Oncol.* **33**, 11–16.
- Sterin-Speziale, N., Kahane, V. L., Setton, C. P., del Carmen Fernandez, M. & Speziale, E. H. (1992) *Lipids* **27**, 10–14.